

# Estimating Astrophysical Population Properties using a multi-component Stochastic Gravitational-Wave Background Search

F. Delillo<sup>\*</sup>, J. Suresh<sup>†</sup>  
*Centre for Cosmology, Particle Physics and Phenomenology (CP3),  
Université catholique de Louvain, Louvain-la-Neuve, B-1348, Belgium*  
(Dated: March 27, 2024)

The recent start of the fourth observing run of the LIGO-Virgo-KAGRA (LVK) collaboration has reopened the hunt for gravitational-wave (GW) signals, with one compact-binary-coalescence (CBC) signal expected to be observed every few days. Among the signals that could be detected for the first time there is the stochastic gravitational-wave background (SGWB) from the superposition of unresolvable GW signals that cannot be detected individually. In fact, multiple SGWBs are likely to arise given the variety of sources, making it crucial to identify the dominant components and assess their origin. However, most search methods with ground-based detectors assume the presence of one SGWB component at a time, which could lead to biased results in estimating its spectral shape if multiple SGWBs exist. Therefore, a joint estimate of the components is necessary. In this work, we adapt such an approach and analyse the data from the first three LVK observing runs, searching for a multi-component isotropic SGWB. We do not find evidence for any SGWB and establish upper limits on the dimensionless energy parameter  $\Omega_{\text{gw}}(f)$  at 25 Hz for five different power-law spectral indices,  $\alpha = 0, 2/3, 2, 3, 4$ , jointly. For the spectral indices  $\alpha = 2/3, 2, 4$ , corresponding to astrophysical SGWBs from CBCs, r-mode instabilities in young rotating neutron stars, and magnetars, we draw further astrophysical implications by constraining the ensemble parameters  $K_{\text{CBC}}$ ,  $K_{\text{r-modes}}$ ,  $K_{\text{magnetars}}$ , defined in the main text.

## I. INTRODUCTION

Gravitational-wave (GW) astronomy has entered a new era with the recent start of the fourth observing run of the LIGO-Virgo-KAGRA (LVK) collaboration. The hunt for gravitational-wave (GW) signals has reopened, with one compact-binary-coalescence (CBC) signal expected to be observed every few days. Among the signals that could be detected for the first time there is the stochastic gravitational-wave background (SGWB) from the superposition of unresolvable GW signals that cannot be detected individually. In fact, multiple SGWBs are likely to arise given the variety of sources, making it crucial to identify the dominant components and assess their origin. However, most search methods with ground-based detectors assume the presence of one SGWB component at a time, which could lead to biased results in estimating its spectral shape if multiple SGWBs exist. Therefore, a joint estimate of the components is necessary. In this work, we adapt such an approach and analyse the data from the first three LVK observing runs, searching for a multi-component isotropic SGWB. We do not find evidence for any SGWB and establish upper limits on the dimensionless energy parameter  $\Omega_{\text{gw}}(f)$  at 25 Hz for five different power-law spectral indices,  $\alpha = 0, 2/3, 2, 3, 4$ , jointly. For the spectral indices  $\alpha = 2/3, 2, 4$ , corresponding to astrophysical SGWBs from CBCs, r-mode instabilities in young rotating neutron stars, and magnetars, we draw further astrophysical implications by constraining the ensemble parameters  $K_{\text{CBC}}$ ,  $K_{\text{r-modes}}$ ,  $K_{\text{magnetars}}$ , defined in the main text.

The recent start of the fourth observing run of the LIGO-Virgo-KAGRA (LVK) collaboration has reopened the hunt for gravitational-wave (GW) signals, with one compact-binary-coalescence (CBC) signal expected to be observed every few days. Among the signals that could be detected for the first time there is the stochastic gravitational-wave background (SGWB) from the superposition of unresolvable GW signals that cannot be detected individually. In fact, multiple SGWBs are likely to arise given the variety of sources, making it crucial to identify the dominant components and assess their origin. However, most search methods with ground-based detectors assume the presence of one SGWB component at a time, which could lead to biased results in estimating its spectral shape if multiple SGWBs exist. Therefore, a joint estimate of the components is necessary. In this work, we adapt such an approach and analyse the data from the first three LVK observing runs, searching for a multi-component isotropic SGWB. We do not find evidence for any SGWB and establish upper limits on the dimensionless energy parameter  $\Omega_{\text{gw}}(f)$  at 25 Hz for five different power-law spectral indices,  $\alpha = 0, 2/3, 2, 3, 4$ , jointly. For the spectral indices  $\alpha = 2/3, 2, 4$ , corresponding to astrophysical SGWBs from CBCs, r-mode instabilities in young rotating neutron stars, and magnetars, we draw further astrophysical implications by constraining the ensemble parameters  $K_{\text{CBC}}$ ,  $K_{\text{r-modes}}$ ,  $K_{\text{magnetars}}$ , defined in the main text.

<sup>\*</sup> federico.delillo@uclouvain.be  
<sup>†</sup> jishnu.suresh@uclouvain.be



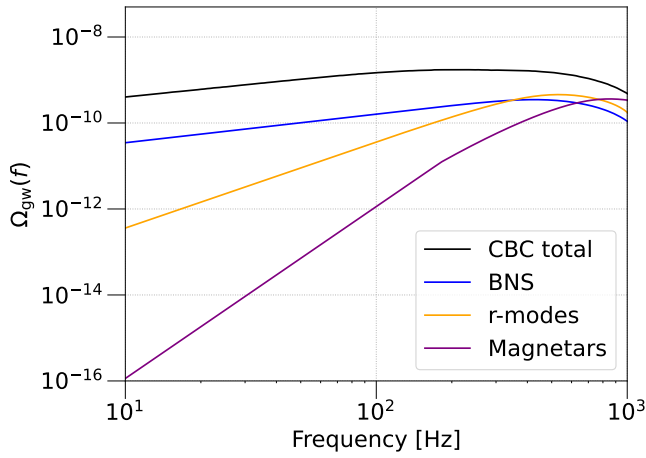


FIG. 1. Landscape plot with the intensity of different astrophysical SGWBs. The black line denotes the median value of the total CBC SGWB as inferred from the GWTC-3 in [8]. The blue line represents the median value of the BNS SGWB, again from [8]. The orange line is the SGWB from r-modes from [20] with our conventions, setting  $K = -5/4$  and further scaling equation (17) to the case where just 1% of the young NSs enters the instability [61]. The purple line is the SGWB from magnetars, using  $\varepsilon = 5 \times 10^{-4}$  and  $B = 10^{11}$  T, with the other parameters from [63].

(2)  $\mathcal{M}_c$

Is  $\mathcal{M}_c$   $\mathcal{M}_c$

$$\frac{dE_{\text{gw}}}{df} = \frac{\pi^{2/3}}{3G} (GM_c)^{5/3} f^{-1/3}. \quad (8)$$

$\mathcal{M}_c$   $\mathcal{M}_c$

$\mathcal{M}_c$   $\mathcal{M}_c$

$\mathcal{M}_c$   $\mathcal{M}_c$

$\mathcal{M}_c$   $\mathcal{M}_c$

$\mathcal{M}_c$   $\mathcal{M}_c$

$\mathcal{M}_c$   $\mathcal{M}_c$

$\mathcal{M}_c$   $\mathcal{M}_c$

$\mathcal{M}_c$   $\mathcal{M}_c$

$\mathcal{M}_c$   $\mathcal{M}_c$

$\mathcal{M}_c$   $\mathcal{M}_c$

$\mathcal{M}_c$   $\mathcal{M}_c$

$$R(z) = \int dt_d R_f(z_f(z, t_d)) P_{t_d}(t_d), \quad (9)$$

$\mathcal{M}_c$   $\mathcal{M}_c$

$\mathcal{M}_c$   $\mathcal{M}_c$

$$\Omega_{\text{gw},j}(f) = \xi_j \left( \frac{f}{f_{\text{ref}}} \right)^{2/3} r_{0,j} \langle \mathcal{M}_c^{5/3} \rangle_j \equiv \xi_j \left( \frac{f}{f_{\text{ref}}} \right)^{2/3} K_j, \quad j = \text{B}, \text{S}, \text{M}, \quad (11)$$

$\mathcal{M}_c$   $\mathcal{M}_c$

$$R_f(z_f) = r_0 \frac{\mathcal{M}_c}{\mathcal{M}_c} z_f \quad (10)$$

$\mathcal{M}_c$   $\mathcal{M}_c$

$\mathcal{M}_c$   $\mathcal{M}_c$

$\mathcal{M}_c$   $\mathcal{M}_c$

$\mathcal{M}_c$   $\mathcal{M}_c$

$\mathcal{M}_c$   $\mathcal{M}_c$

$\mathcal{M}_c$   $\mathcal{M}_c$

$\mathcal{M}_c$   $\mathcal{M}_c$

$\mathcal{M}_c$   $\mathcal{M}_c$

$\mathcal{M}_c$   $\mathcal{M}_c$

$\mathcal{M}_c$   $\mathcal{M}_c$

$\mathcal{M}_c$   $\mathcal{M}_c$

$\mathcal{M}_c$   $\mathcal{M}_c$

$\mathcal{M}_c$   $\mathcal{M}_c$

$\mathcal{M}_c$   $\mathcal{M}_c$

$\mathcal{M}_c$   $\mathcal{M}_c$

$\mathcal{M}_c$   $\mathcal{M}_c$

$\mathcal{M}_c$   $\mathcal{M}_c$

$\mathcal{M}_c$   $\mathcal{M}_c$

$\mathcal{M}_c$   $\mathcal{M}_c$

$\mathcal{M}_c$   $\mathcal{M}_c$

$\mathcal{M}_c$   $\mathcal{M}_c$

$\mathcal{M}_c$   $\mathcal{M}_c$

$\mathcal{M}_c$   $\mathcal{M}_c$

$\mathcal{M}_c$   $\mathcal{M}_c$

$\mathcal{M}_c$   $\mathcal{M}_c$

$\mathcal{M}_c$   $\mathcal{M}_c$

$\mathcal{M}_c$   $\mathcal{M}_c$

$\mathcal{M}_c$   $\mathcal{M}_c$

$\mathcal{M}_c$   $\mathcal{M}_c$

$\mathcal{M}_c$   $\mathcal{M}_c$

$\mathcal{M}_c$   $\mathcal{M}_c$

$\mathcal{M}_c$   $\mathcal{M}_c$

$\mathcal{M}_c$   $\mathcal{M}_c$

$\mathcal{M}_c$   $\mathcal{M}_c$

$\mathcal{M}_c$   $\mathcal{M}_c$

$\mathcal{M}_c$   $\mathcal{M}_c$

$\mathcal{M}_c$   $\mathcal{M}_c$

$\mathcal{M}_c$   $\mathcal{M}_c$

$\mathcal{M}_c$   $\mathcal{M}_c$

$\mathcal{M}_c$   $\mathcal{M}_c$

$\mathcal{M}_c$   $\mathcal{M}_c$

$\mathcal{M}_c$   $\mathcal{M}_c$

$\mathcal{M}_c$   $\mathcal{M}_c$

$\mathcal{M}_c$   $\mathcal{M}_c$

$\mathcal{M}_c$   $\mathcal{M}_c$

$\mathcal{M}_c$   $\mathcal{M}_c$

$\mathcal{M}_c$   $\mathcal{M}_c$

$\mathcal{M}_c$   $\mathcal{M}_c$

$\mathcal{M}_c$   $\mathcal{M}_c$

$\mathcal{M}_c$   $\mathcal{M}_c$

$\mathcal{M}_c$   $\mathcal{M}_c$

$\mathcal{M}_c$   $\mathcal{M}_c$

$\mathcal{M}_c$   $\mathcal{M}_c$

$\mathcal{M}_c$   $\mathcal{M}_c$

$\mathcal{M}_c$   $\mathcal{M}_c$

$\mathcal{M}_c$   $\mathcal{M}_c$

$$p_{t_d} \propto t_d^{-1} \mathcal{M}_c$$

$$Z < 0.1 Z_\odot$$

$$m_1 \text{ and } m_2$$

$$M_\odot.$$





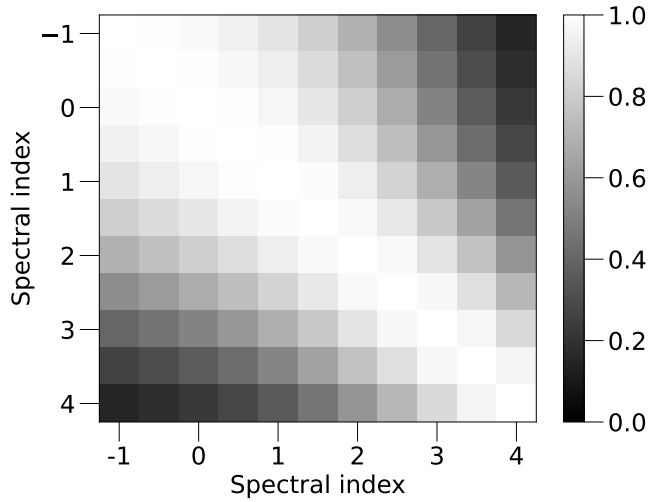


FIG. 2. Preconditioned Fisher matrix for data from the first three LVK observing runs, showing the couplings among different spectral indices. The diagonal is unity by construction, with the off-diagonal element being smaller than one and positive.

$$\hat{\Omega} = \Gamma^{-1} \cdot \mathbf{X}, \quad (22)$$

$$\mathcal{L}(\hat{\Omega}_\alpha | \Omega_\alpha) = \frac{1}{(2\pi)^{N/2} (\det \Sigma)^{1/2}} \exp \left[ -\frac{1}{2} (\hat{\Omega}_\alpha - \Omega_\alpha) \Sigma_{\alpha\alpha'}^{-1} (\hat{\Omega}_{\alpha'} - \Omega_{\alpha'}) \right]. \quad (23)$$

$$\Omega_\alpha = \xi_\alpha \prod_i \langle \theta_i^{c_i} \rangle. \quad (24)$$

$$X_\alpha = \Delta f \sum_{I>J} \sum_{f,t} \frac{\gamma_{IJ}(f) S_0(f) \tilde{s}_I^*(t; f) \tilde{s}_J(t; f)}{P_I(t; f) P_J(t; f)} w_\alpha(f),$$

$$\Gamma_{\alpha\alpha'} = T \Delta f \sum_{I>J} \sum_{f,t} \frac{\gamma_{IJ}^2(f) S_0^2(f)}{P_I(t; f) P_J(t; f)} w_\alpha(f) w_{\alpha'}(f), \quad (23)$$

$$P_I(t; f) = \int_{-\infty}^{\infty} dt' \tilde{s}_I(t-t'; f) \tilde{s}_I^*(t-t'; f),$$

$$\Gamma_{\alpha\alpha'} = \int_{-\infty}^{\infty} dt \int_{-\infty}^{\infty} dt' \Gamma_{\alpha\alpha'}(t, t').$$

$$\Gamma \equiv \Gamma'_{\alpha\alpha'} = \frac{\Gamma_{\alpha\alpha'}}{\sqrt{\Gamma_\alpha \Gamma_{\alpha'}}}, \quad (24)$$

$$\hat{\Omega}_\alpha \equiv \hat{\Omega}'_{\alpha\alpha'} = \frac{X'_\alpha}{\sqrt{\Gamma_\alpha}}, \quad (25)$$

$$X'_\alpha = X_\alpha / \sqrt{\Gamma_\alpha},$$

$$\Sigma_{\alpha\alpha'} = \frac{(\Gamma'_{\alpha\alpha'})^{-1}}{\sqrt{\Gamma_\alpha \Gamma_{\alpha'}}}, \quad (26)$$

$$\sigma_\alpha = \left[ \sqrt{\det \Sigma} \quad \beta_{\beta'} \right]_\alpha. \quad (27)$$

## IV. RESULTS AND DISCUSSIONS

$$\vec{\alpha} = \{0, 2/3, 2, 3, 4\}$$

### A. Power law energy density spectrum



	$\hat{\Omega}_0$	$\hat{\Omega}_{2/3}$	$\hat{\Omega}_2$	$\hat{\Omega}_3$	$\hat{\Omega}_4$
$\alpha = \{0\}$	$(1.5 \pm 7.5) \times 10^{-9}$	-	-	-	-
$\alpha = \{2/3\}$	-	$(2.3 \pm 56.2) \times 10^{-10}$	-	-	-
$\alpha = \{2\}$	-	-	$(-1.3 \pm 2.5) \times 10^{-9}$	-	-
$\alpha = \{3\}$	-	-	-	$(-9.8 \pm 10.3) \times 10^{-10}$	-
$\alpha = \{4\}$	-	-	-	-	$(-4.0 \pm 3.4) \times 10^{-10}$
$\alpha = \{0, 2/3\}$	$(4.4 \pm 4.6) \times 10^{-8}$	$(-3.2 \pm 3.4) \times 10^{-8}$	-	-	-
$\alpha = \{0, 2\}$	$(1.6 \pm 1.4) \times 10^{-8}$	-	$(-5.8 \pm 4.6) \times 10^{-9}$	-	-
$\alpha = \{0, 3\}$	$(9.5 \pm 9.5) \times 10^{-9}$	-	-	$(-1.8 \pm 1.3) \times 10^{-9}$	-
$\alpha = \{0, 4\}$	$(6.1 \pm 8.2) \times 10^{-9}$	-	-	-	$(-5.1 \pm 3.7) \times 10^{-10}$
$\alpha = \{2/3, 2\}$	-	$(1.7 \pm 1.4) \times 10^{-8}$	$(-8.3 \pm 6.1) \times 10^{-9}$	-	-
$\alpha = \{2/3, 3\}$	-	$(8.4 \pm 8.1) \times 10^{-9}$	-	$(-2.1 \pm 1.5) \times 10^{-9}$	-
$\alpha = \{2/3, 4\}$	-	$(5.0 \pm 6.6) \times 10^{-9}$	-	-	$(-5.6 \pm 4.0) \times 10^{-10}$
$\alpha = \{2, 3\}$	-	-	$(7.6 \pm 7.2) \times 10^{-9}$	$(-3.9 \pm 2.9) \times 10^{-9}$	-
$\alpha = \{2, 4\}$	-	-	$(3.1 \pm 4.3) \times 10^{-9}$	-	$(-7.4 \pm 5.8) \times 10^{-10}$
$\alpha = \{3, 4\}$	-	-	-	$(2.4 \pm 3.7) \times 10^{-9}$	$(-1.2 \pm 1.2) \times 10^{-9}$
$\alpha = \{0, 2/3, 2\}$	$(-7.9 \pm 11.4) \times 10^{-8}$	$(9.5 \pm 11.3) \times 10^{-8}$	$(-1.8 \pm 1.5) \times 10^{-8}$	-	-
$\alpha = \{0, 2/3, 3\}$	$(-3.2 \pm 8.3) \times 10^{-8}$	$(3.5 \pm 7.0) \times 10^{-8}$	-	$(-2.9 \pm 2.7) \times 10^{-9}$	-
$\alpha = \{0, 2/3, 4\}$	$(-9.9 \pm 69.8) \times 10^{-9}$	$(1.3 \pm 5.6) \times 10^{-8}$	-	-	$(-6.2 \pm 6.1) \times 10^{-10}$
$\alpha = \{0, 2, 3\}$	$(-1.0 \pm 30.0) \times 10^{-9}$	-	$(8.3 \pm 22.6) \times 10^{-9}$	$(-4.1 \pm 6.4) \times 10^{-9}$	-
$\alpha = \{0, 2, 4\}$	$(4.3 \pm 25.0) \times 10^{-9}$	-	$(1.0 \pm 12.9) \times 10^{-9}$	-	$(-5.9 \pm 10.5) \times 10^{-10}$
$\alpha = \{0, 3, 4\}$	$(6.5 \pm 17.8) \times 10^{-9}$	-	-	$(-1.8 \pm 81.2) \times 10^{-10}$	$(-4.6 \pm 23.2) \times 10^{-10}$
$\alpha = \{2/3, 2, 3\}$	-	$(1.7 \pm 38.8) \times 10^{-9}$	$(6.1 \pm 34.4) \times 10^{-9}$	$(-3.6 \pm 8.4) \times 10^{-9}$	-
$\alpha = \{2/3, 2, 4\}$	-	$(7.7 \pm 30.1) \times 10^{-9}$	$(-1.7 \pm 19.5) \times 10^{-9}$	-	$(-4.5 \pm 12.7) \times 10^{-10}$
$\alpha = \{2/3, 3, 4\}$	-	$(8.1 \pm 18.3) \times 10^{-9}$	-	$(-1.9 \pm 10.4) \times 10^{-9}$	$(-5.6 \pm 280.6) \times 10^{-11}$
$\alpha = \{2, 3, 4\}$	-	-	$(1.6 \pm 2.8) \times 10^{-8}$	$(-1.1 \pm 2.5) \times 10^{-8}$	$(1.5 \pm 4.9) \times 10^{-9}$
$\alpha = \{0, 2/3, 2, 3\}$	$(-3.2 \pm 3.5) \times 10^{-7}$	$(4.1 \pm 4.6) \times 10^{-7}$	$(-1.2 \pm 1.5) \times 10^{-7}$	$(1.9 \pm 2.6) \times 10^{-8}$	-
$\alpha = \{0, 2/3, 2, 4\}$	$(-2.5 \pm 2.7) \times 10^{-7}$	$(3.0 \pm 3.3) \times 10^{-7}$	$(-6.8 \pm 7.6) \times 10^{-8}$	-	$(2.1 \pm 3.1) \times 10^{-9}$
$\alpha = \{0, 2/3, 3, 4\}$	$(-1.5 \pm 1.8) \times 10^{-7}$	$(1.6 \pm 1.9) \times 10^{-7}$	-	$(-2.3 \pm 2.8) \times 10^{-8}$	$(4.5 \pm 6.3) \times 10^{-9}$
$\alpha = \{0, 2, 3, 4\}$	$(-4.0 \pm 6.3) \times 10^{-8}$	-	$(7.6 \pm 9.9) \times 10^{-8}$	$(-4.7 \pm 6.2) \times 10^{-8}$	$(7.1 \pm 10.2) \times 10^{-9}$
$\alpha = \{2/3, 2, 3, 4\}$	-	$(-5.5 \pm 9.6) \times 10^{-8}$	$(9.9 \pm 14.7) \times 10^{-8}$	$(-5.4 \pm 7.8) \times 10^{-8}$	$(7.8 \pm 12.0) \times 10^{-9}$
$\alpha = \{0, 2/3, 2, 3, 4\}$	$(-6.9 \pm 8.9) \times 10^{-7}$	$(9.8 \pm 13.6) \times 10^{-7}$	$(-4.3 \pm 7.1) \times 10^{-7}$	$(1.3 \pm 2.6) \times 10^{-7}$	$(-1.4 \pm 3.0) \times 10^{-8}$

TABLE I. Estimators from the multi-components analysis in the 20-100 Hz band for the different combinations of the five spectral indices. Horizontal lines divide the table in regions where a fixed number of components is considered for the analysis.

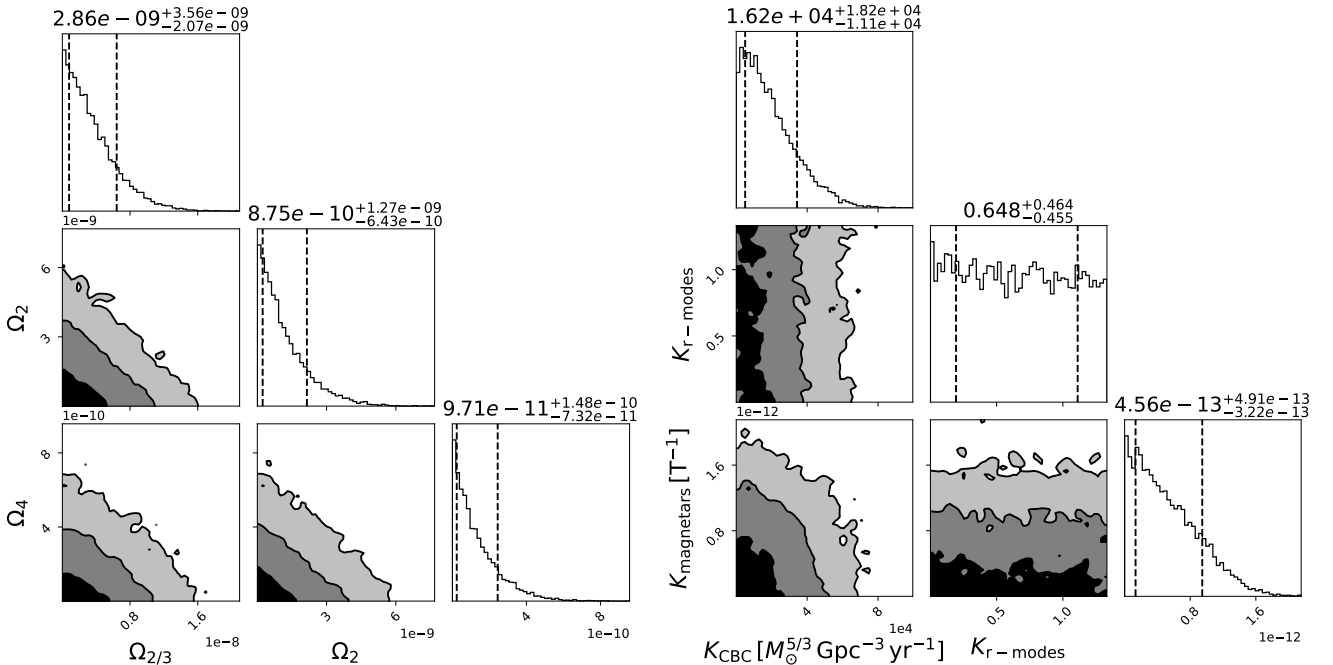


FIG. 3. Results of the parameter estimation for the  $\alpha = 2/3, 2, 4$  combination in the 20 – 100 Hz band for power-law  $\Omega_\alpha$  (left panel) and the corresponding astrophysical parameters (right panel). Contour plots show the  $1\sigma$ ,  $2\sigma$ , and  $3\sigma$  credible areas (black, grey, light grey, respectively). The dashed black lines in the histogram panels delimit the  $1\sigma$  region of the estimated parameters.







- tal monitors, and the geophysics interferometer, PTEP **2021**, 05A102 (2021), arXiv:2009.09305 [gr-qc].
- [6] M. S. et al., The science case for LIGO-india, *Classical and Quantum Gravity* **39**, 025004 (2021).
- [7] R. Abbott *et al.* (LIGO Scientific, VIRGO, KAGRA), GWTC-3: Compact Binary Coalescences Observed by LIGO and Virgo During the Second Part of the Third Observing Run (2021), arXiv:2111.03606 [gr-qc].
- [8] R. Abbott *et al.* (KAGRA, VIRGO, LIGO Scientific), Population of Merging Compact Binaries Inferred Using Gravitational Waves through GWTC-3, *Phys. Rev. X* **13**, 011048 (2023), arXiv:2111.03634 [astro-ph.HE].
- [9] R. W. Kiendrebeogo *et al.*, Updated observing scenarios and multi-messenger implications for the International Gravitational-wave Network's O4 and O5 (2023), arXiv:2306.09234 [astro-ph.HE].
- [10] P. A. Rosado, Gravitational wave background from binary systems, *Phys. Rev. D* **84**, 084004 (2011), arXiv:1106.5795 [gr-qc].
- [11] X.-J. Zhu, E. Howell, T. Regimbau, D. Blair, and Z.-H. Zhu, Stochastic Gravitational Wave Background from Coalescing Binary Black Holes, *Astrophys. J.* **739**, 86 (2011), arXiv:1104.3565 [gr-qc].
- [12] S. Marassi, R. Schneider, G. Corvino, V. Ferrari, and S. Portegies Zwart, Imprint of the merger and ring-down on the gravitational wave background from black hole binaries coalescence, *Phys. Rev. D* **84**, 124037 (2011), arXiv:1111.6125 [astro-ph.CO].
- [13] C. Wu, V. Mandic, and T. Regimbau, Accessibility of the Gravitational-Wave Background due to Binary Coalescences to Second and Third Generation Gravitational-Wave Detectors, *Phys. Rev. D* **85**, 104024 (2012), arXiv:1112.1898 [gr-qc].
- [14] X.-J. Zhu, E. J. Howell, D. G. Blair, and Z.-H. Zhu, On the gravitational wave background from compact binary coalescences in the band of ground-based interferometers, *Mon. Not. Roy. Astron. Soc.* **431**, 882 (2013), arXiv:1209.0595 [gr-qc].
- [15] P. A. Rosado, Gravitational wave background from rotating neutron stars, *Phys. Rev. D* **86**, 104007 (2012), arXiv:1206.1330 [gr-qc].
- [16] T. Regimbau and J. A. de Freitas Pacheco, Cosmic background of gravitational waves from rotating neutron stars, *Astron. Astrophys.* **376**, 381 (2001), arXiv:astro-ph/0105260.
- [17] S. Marassi, R. Ciolfi, R. Schneider, L. Stella, and V. Ferrari, Stochastic background of gravitational waves emitted by magnetars, *Mon. Not. Roy. Astron. Soc.* **411**, 2549 (2011), arXiv:1009.1240 [astro-ph.CO].
- [18] C.-J. Wu, V. Mandic, and T. Regimbau, Accessibility of the stochastic gravitational wave background from magnetars to the interferometric gravitational wave detectors, *Phys. Rev. D* **87**, 042002 (2013).
- [19] V. Ferrari, S. Matarrese, and R. Schneider, Stochastic background of gravitational waves generated by a cosmological population of young, rapidly rotating neutron stars, *Mon. Not. Roy. Astron. Soc.* **303**, 258 (1999), arXiv:astro-ph/9806357.
- [20] X.-J. Zhu, X.-L. Fan, and Z.-H. Zhu, Stochastic Gravitational Wave Background from Neutron Star r-mode Instability Revisited, *Astrophys. J.* **729**, 59 (2011), arXiv:1102.2786 [astro-ph.CO].
- [21] P. D. Lasky, M. F. Bennett, and A. Melatos, Stochastic gravitational wave background from hydrodynamic turbulence in differentially rotating neutron stars, *Phys. Rev. D* **87**, 063004 (2013), arXiv:1302.6033 [astro-ph.HE].
- [22] A. Buonanno, G. Sigl, G. G. Raffelt, H.-T. Janka, and E. Muller, Stochastic gravitational wave background from cosmological supernovae, *Phys. Rev. D* **72**, 084001 (2005), arXiv:astro-ph/0412277.
- [23] E. Howell, D. Coward, R. Burman, D. Blair, and J. Gilmore, The gravitational wave background from neutron star birth throughout the cosmos, *mnras* **351**, 1237 (2004).
- [24] P. Sandick, K. A. Olive, F. Daigne, and E. Vangioni, Gravitational Waves from the First Stars, *Phys. Rev. D* **73**, 104024 (2006), arXiv:astro-ph/0603544.
- [25] S. Marassi, R. Schneider, and V. Ferrari, Gravitational wave backgrounds and the cosmic transition from Population III to Population II stars, *Mon. Not. Roy. Astron. Soc.* **398**, 293 (2009), arXiv:0906.0461 [astro-ph.CO].
- [26] X.-J. Zhu, E. Howell, and D. Blair, Observational upper limits on the gravitational wave production of core collapse supernovae, *Mon. Not. Roy. Astron. Soc.* **409**, L132 (2010), arXiv:1008.0472 [gr-qc].
- [27] V. Ferrari, S. Matarrese, and R. Schneider, Gravitational wave background from a cosmological population of core collapse supernovae, *Mon. Not. Roy. Astron. Soc.* **303**, 247 (1999), arXiv:astro-ph/9804259.
- [28] K. Crocker, V. Mandic, T. Regimbau, K. Belczynski, W. Gladysz, K. Olive, T. Prestegard, and E. Vangioni, Model of the stochastic gravitational-wave background due to core collapse to black holes, *Phys. Rev. D* **92**, 063005 (2015), arXiv:1506.02631 [gr-qc].
- [29] K. Crocker, T. Prestegard, V. Mandic, T. Regimbau, K. Olive, and E. Vangioni, Systematic study of the stochastic gravitational-wave background due to stellar core collapse, *Phys. Rev. D* **95**, 063015 (2017), arXiv:1701.02638 [astro-ph.CO].
- [30] T. W. B. Kibble, Topology of Cosmic Domains and Strings, *J. Phys. A* **9**, 1387 (1976).
- [31] S. Sarangi and S. H. H. Tye, Cosmic string production towards the end of brane inflation, *Phys. Lett. B* **536**, 185 (2002), arXiv:hep-th/0204074.
- [32] T. Damour and A. Vilenkin, Gravitational radiation from cosmic (super)strings: Bursts, stochastic background, and observational windows, *Phys. Rev. D* **71**, 063510 (2005), arXiv:hep-th/0410222.
- [33] X. Siemens, V. Mandic, and J. Creighton, Gravitational wave stochastic background from cosmic (super)strings, *Phys. Rev. Lett.* **98**, 111101 (2007), arXiv:astro-ph/0610920.
- [34] L. Marzola, A. Racioppi, and V. Vaskonen, Phase transition and gravitational wave phenomenology of scalar conformal extensions of the Standard Model, *Eur. Phys. J. C* **77**, 484 (2017), arXiv:1704.01034 [hep-ph].
- [35] B. Von Harling, A. Pomarol, O. Pujolàs, and F. Rompineve, Peccei-Quinn Phase Transition at LIGO, *JHEP* **04**, 195, arXiv:1912.07587 [hep-ph].
- [36] V. Mandic, S. Bird, and I. Cholis, Stochastic Gravitational-Wave Background due to Primordial Binary Black Hole Mergers, *Phys. Rev. Lett.* **117**, 201102 (2016), arXiv:1608.06699 [astro-ph.CO].
- [37] S. Clesse, J. García-Bellido, and S. Orani, Detecting the Stochastic Gravitational Wave Background from Primordial Black Hole Formation (2018), arXiv:1812.11011 [astro-ph.CO].

- [38] E. Bagui and S. Clesse, A boosted gravitational wave background for primordial black holes with broad mass distributions and thermal features, *Phys. Dark Univ.* **38**, 101115 (2022), arXiv:2110.07487 [astro-ph.CO].
- [39] S. Mukherjee, M. S. P. Meinema, and J. Silk, Prospects of discovering subsolar primordial black holes using the stochastic gravitational wave background from third-generation detectors, *Mon. Not. Roy. Astron. Soc.* **510**, 6218 (2022), arXiv:2107.02181 [astro-ph.CO].
- [40] S. Mukherjee and J. Silk, Can we distinguish astrophysical from primordial black holes via the stochastic gravitational wave background?, *Mon. Not. Roy. Astron. Soc.* **506**, 3977 (2021), arXiv:2105.11139 [gr-qc].
- [41] X. Martin and A. Vilenkin, Gravitational wave background from hybrid topological defects, *Phys. Rev. Lett.* **77**, 2879 (1996), arXiv:astro-ph/9606022.
- [42] H. An and C. Yang, Gravitational Waves Produced by Domain Walls During Inflation (2023), arXiv:2304.02361 [hep-ph].
- [43] A. A. Starobinskiĭ, Spectrum of relict gravitational radiation and the early state of the universe, *Soviet Journal of Experimental and Theoretical Physics Letters* **30**, 682 (1979).
- [44] R. Bar-Kana, Limits on direct detection of gravitational waves, *Phys. Rev. D* **50**, 1157 (1994), arXiv:astro-ph/9401050.
- [45] M. S. Turner, Detectability of inflation produced gravitational waves, *Phys. Rev. D* **55**, R435 (1997), arXiv:astro-ph/9607066.
- [46] M. Gasperini and G. Veneziano, Pre - big bang in string cosmology, *Astropart. Phys.* **1**, 317 (1993), arXiv:hep-th/9211021.
- [47] V. Mandic and A. Buonanno, Accessibility of the pre-big-bang models to ligo, *Phys. Rev. D* **73**, 063008 (2006), arXiv:astro-ph/0510341.
- [48] M. Gasperini, Observable gravitational waves in pre-big bang cosmology: an update, *JCAP* **12**, 010, arXiv:1606.07889 [gr-qc].
- [49] G. Agazie *et al.* (NANOGrav), The NANOGrav 15 yr Data Set: Evidence for a Gravitational-wave Background, *Astrophys. J. Lett.* **951**, L8 (2023), arXiv:2306.16213 [astro-ph.HE].
- [50] J. Antoniadis *et al.*, The second data release from the European Pulsar Timing Array III. Search for gravitational wave signals (2023), arXiv:2306.16214 [astro-ph.HE].
- [51] D. J. Reardon *et al.*, Search for an Isotropic Gravitational-wave Background with the Parkes Pulsar Timing Array, *Astrophys. J. Lett.* **951**, L6 (2023), arXiv:2306.16215 [astro-ph.HE].
- [52] H. Xu *et al.*, Searching for the Nano-Hertz Stochastic Gravitational Wave Background with the Chinese Pulsar Timing Array Data Release I, *Res. Astron. Astrophys.* **23**, 075024 (2023), arXiv:2306.16216 [astro-ph.HE].
- [53] C. Ungarelli and A. Vecchio, Studying the anisotropy of the gravitational wave stochastic background with LISA, *Phys. Rev. D* **64**, 121501 (2001), arXiv:astro-ph/0106538.
- [54] V. Mandic, E. Thrane, S. Giampanis, and T. Regimbau, Parameter Estimation in Searches for the Stochastic Gravitational-Wave Background, *Phys. Rev. Lett.* **109**, 171102 (2012), arXiv:1209.3847 [astro-ph.CO].
- [55] K. Martinovic, P. M. Meyers, M. Sakellariadou, and N. Christensen, Simultaneous estimation of astrophysical and cosmological stochastic gravitational-wave backgrounds with terrestrial detectors, *Phys. Rev. D* **103**, 043023 (2021), arXiv:2011.05697 [gr-qc].
- [56] A. Parida, S. Mitra, and S. Jhingan, Component Separation of a Isotropic Gravitational Wave Background, *JCAP* **04**, 024, arXiv:1510.07994 [astro-ph.CO].
- [57] J. Suresh, D. Agarwal, and S. Mitra, Jointly setting upper limits on multiple components of an anisotropic stochastic gravitational-wave background, *Phys. Rev. D* **104**, 102003 (2021), arXiv:2106.09593 [gr-qc].
- [58] G. Boileau, A. Lamberts, N. J. Cornish, and R. Meyer, Spectral separation of the stochastic gravitational-wave background for LISA in the context of a modulated Galactic foreground, *Mon. Not. Roy. Astron. Soc.* **508**, 803 (2021), [Erratum: *Mon. Not. Roy. Astron. Soc.* 508, 5554–5555 (2021)], arXiv:2105.04283 [gr-qc].
- [59] B. Allen and J. D. Romano, Detecting a stochastic background of gravitational radiation: Signal processing strategies and sensitivities, *Phys. Rev. D* **59**, 102001 (1999), arXiv:gr-qc/9710117.
- [60] E. S. Phinney, A Practical theorem on gravitational wave backgrounds (2001), arXiv:astro-ph/0108028.
- [61] T. Regimbau, The astrophysical gravitational wave stochastic background, *Res. Astron. Astrophys.* **11**, 369 (2011), arXiv:1101.2762 [astro-ph.CO].
- [62] T. Regimbau, The Quest for the Astrophysical Gravitational-Wave Background with Terrestrial Detectors, *Symmetry* **14**, 270 (2022).
- [63] T. Regimbau and V. Mandic, Astrophysical Sources of Stochastic Gravitational-Wave Background, *Class. Quant. Grav.* **25**, 184018 (2008), arXiv:0806.2794 [astro-ph].
- [64] L. Lehoucq, I. Dvorkin, R. Srinivasan, C. Pellouin, and A. Lamberts, Astrophysical Uncertainties in the Gravitational-Wave Background from Stellar-Mass Compact Binary Mergers (2023), arXiv:2306.09861 [astro-ph.HE].
- [65] P. Ajith *et al.*, A Template bank for gravitational waveforms from coalescing binary black holes. I. Non-spinning binaries, *Phys. Rev. D* **77**, 104017 (2008), [Erratum: *Phys. Rev. D* 79, 129901 (2009)], arXiv:0710.2335 [gr-qc].
- [66] P. Ajith *et al.*, Inspiral-merger-ringdown waveforms for black-hole binaries with non-precessing spins, *Phys. Rev. Lett.* **106**, 241101 (2011), arXiv:0909.2867 [gr-qc].
- [67] E. Vangioni, K. A. Olive, T. Prestegard, J. Silk, P. Petitjean, and V. Mandic, The Impact of Star Formation and Gamma-Ray Burst Rates at High Redshift on Cosmic Chemical Evolution and Reionization, *Mon. Not. Roy. Astron. Soc.* **447**, 2575 (2015), arXiv:1409.2462 [astro-ph.GA].
- [68] M. Chruslinska, K. Belczynski, J. Klencki, and M. Benacquista, Double neutron stars: merger rates revisited, *Mon. Not. Roy. Astron. Soc.* **474**, 2937 (2018), arXiv:1708.07885 [astro-ph.HE].
- [69] M. Mapelli, N. Giacobbo, F. Santoliquido, and M. C. Artale, The properties of merging black holes and neutron stars across cosmic time, *Mon. Not. Roy. Astron. Soc.* **487**, 2 (2019), arXiv:1902.01419 [astro-ph.HE].
- [70] M. Chruslinska, G. Nelemans, and K. Belczynski, The influence of the distribution of cosmic star formation at different metallicities on the properties of merging double compact objects, *Mon. Not. Roy. Astron. Soc.* **482**, 5012 (2019), arXiv:1811.03565 [astro-ph.HE].
- [71] F. Santoliquido, M. Mapelli, N. Giacobbo, Y. Bouffanais, and M. C. Artale, The cosmic merger rate density of compact objects: impact of star formation, metallicity, ini-

- tial mass function and binary evolution, *Mon. Not. Roy. Astron. Soc.* **502**, 4877 (2021), arXiv:2009.03911 [astro-ph.HE].
- [72] R. C. Duncan and C. Thompson, Formation of Very Strongly Magnetized Neutron Stars: Implications for Gamma-Ray Bursts, *apjl* **392**, L9 (1992).
- [73] S. A. Olausen and V. M. Kaspi, The McGill Magnetar Catalog, *Astrophys. J. Suppl.* **212**, 6 (2014), arXiv:1309.4167 [astro-ph.HE].
- [74] S. Bonazzola and E.ourgoulhon, Gravitational waves from pulsars: Emission by the magnetic field induced distortion, *Astron. Astrophys.* **312**, 675 (1996), arXiv:astro-ph/9602107.
- [75] J. Braithwaite and H. C. Spruit, Structure of the magnetic fields in A stars and white dwarfs, *Nature* **431**, 819 (2004), arXiv:astro-ph/0502043.
- [76] L. Stella, S. Dall’Osso, G. Israel, and A. Vecchio, Gravitational radiation from newborn magnetars, *Astrophys. J. Lett.* **634**, L165 (2005), arXiv:astro-ph/0511068.
- [77] N. Andersson, A New class of unstable modes of rotating relativistic stars, *Astrophys. J.* **502**, 708 (1998), arXiv:gr-qc/9706075.
- [78] J. L. Friedman and S. M. Morsink, Axial instability of rotating relativistic stars, *Astrophys. J.* **502**, 714 (1998), arXiv:gr-qc/9706073.
- [79] B. J. Owen, L. Lindblom, C. Cutler, B. F. Schutz, A. Vecchio, and N. Andersson, Gravitational waves from hot young rapidly rotating neutron stars, *Phys. Rev. D* **58**, 084020 (1998), arXiv:gr-qc/9804044.
- [80] P. M. Sa and B. Tome, The Influence of differential rotation on the detectability of gravitational waves from the r-mode instability, *Phys. Rev. D* **74**, 044011 (2006), arXiv:gr-qc/0606001.
- [81] S. Drasco and E. E. Flanagan, Detection methods for nonGaussian gravitational wave stochastic backgrounds, *Phys. Rev. D* **67**, 082003 (2003), arXiv:gr-qc/0210032.
- [82] R. Abbott *et al.* (LIGO Scientific, Virgo), Open data from the first and second observing runs of Advanced LIGO and Advanced Virgo, *SoftwareX* **13**, 100658 (2021), arXiv:1912.11716 [gr-qc].
- [83] R. Abbott *et al.* (KAGRA, VIRGO, LIGO Scientific), Open Data from the Third Observing Run of LIGO, Virgo, KAGRA, and GEO, *Astrophys. J. Suppl.* **267**, 29 (2023), arXiv:2302.03676 [gr-qc].
- [84] R. Abbott *et al.* (KAGRA, Virgo, LIGO Scientific), Upper limits on the isotropic gravitational-wave background from Advanced LIGO and Advanced Virgo’s third observing run, *Phys. Rev. D* **104**, 022004 (2021), arXiv:2101.12130 [gr-qc].
- [85] R. Abbott *et al.* (LIGO Scientific, VIRGO, KAGRA), Data for Upper Limits on the Isotropic Gravitational-Wave Background from Advanced LIGO’s and Advanced Virgo’s Third Observing Run (2021).
- [86] <https://git.ligo.org/stochastic-public/stochastic>.
- [87] N. Christensen, Measuring the stochastic gravitational-radiation background with laser-interferometric antennas, *Phys. Rev. D* **46**, 5250 (1992).
- [88] E. E. Flanagan, Sensitivity of the laser interferometer gravitational wave observatory to a stochastic background, and its dependence on the detector orientations, *Phys. Rev. D* **48**, 2389 (1993).
- [89] B. P. Abbott *et al.* (LIGO Scientific, Virgo), Search for Tensor, Vector, and Scalar Polarizations in the Stochastic Gravitational-Wave Background, *Phys. Rev. Lett.* **120**, 201102 (2018), arXiv:1802.10194 [gr-qc].
- [90] F. De Lillo, J. Suresh, and A. L. Miller, Stochastic gravitational-wave background searches and constraints on neutron-star ellipticity, *Mon. Not. Roy. Astron. Soc.* **513**, 1105 (2022), arXiv:2203.03536 [gr-qc].
- [91] F. De Lillo, J. Suresh, A. Depasse, M. Sieniawska, A. L. Miller, and G. Bruno, Probing ensemble properties of vortex-avalanche pulsar glitches with a stochastic gravitational-wave background search, *Phys. Rev. D* **107**, 102001 (2023), arXiv:2211.16857 [gr-qc].
- [92] D. Agarwal, J. Suresh, V. Mandic, A. Matas, and T. Regimbau, Targeted search for the stochastic gravitational-wave background from the galactic millisecond pulsar population, *Phys. Rev. D* **106**, 043019 (2022), arXiv:2204.08378 [gr-qc].
- [93] S. van der Walt, S. C. Colbert, and G. Varoquaux, The numpy array: A structure for efficient numerical computation, *Computing in Science Engineering* **13**, 22 (2011).
- [94] P. Virtanen *et al.*, Scipy 1.0: fundamental algorithms for scientific computing in python, *Nature Methods* **17**, 261 (2020).
- [95] J. D. Hunter, Matplotlib: A 2d graphics environment, *Computing in Science & Engineering* **9**, 90 (2007).
- [96] D. Phan, N. Pradhan, and M. Jankowiak, Composable effects for flexible and accelerated probabilistic programming in numpyro, arXiv preprint arXiv:1912.11554 (2019).

## Appendix A: Injection studies

### The data

The data is a set of 1000 realizations of a stochastic background, each of length 1000000 samples. The data is stored in a file named `stochastic_data.npy` in the `stochastic-public` repository.

### 1. Power-law injections: five equal-intensity SGWBs

The data is a set of 1000 realizations of a stochastic background, each of length 1000000 samples. The data is stored in a file named `stochastic_data.npy` in the `stochastic-public` repository.

$$\{\Omega_\alpha = 1 \times 10^{-6}, \alpha \in \{0, 2/3, 2, 3, 4\}\} \text{ at } -126 \text{ H}$$

$$\alpha \in \{0, 2/3, 2, 3, 4\}$$

$$\alpha \in \{0, 2/3, 2, 3, 4\}$$

a. Signal-only case using O3 sensitivity

where  $\Omega_{\alpha}$  and  $\Omega_{\alpha_m}$  are the power-law injection amplitudes for the  $\alpha$  and  $\alpha_m$  components, respectively, and  $w_{\alpha}$  and  $w_{\alpha_m}$  are the corresponding weight functions.

The total power-law injection spectrum is then given by

$$\Omega_{\text{gw}}(f) = \sum_A \Omega_A w_A(f) = \sum_{\alpha} \Omega_{\alpha} w_{\alpha}(f) + \sum_{\alpha_m} \Omega_{\alpha_m} w_{\alpha_m}(f). \quad (A)$$

$$\langle \hat{\Omega}_A \rangle = \Omega_A \cdot \text{Tr} \left[ (\Gamma^{-1})_{AA'} X_{A'} \right], \quad (B)$$

$$\hat{\Omega}_{\alpha}^{(\text{unbiased})} = (\Gamma^{-1})_{\alpha\alpha'} X_{\alpha'} - (\Gamma^{-1})_{\alpha\alpha'} \Gamma_{\alpha'\alpha'_m} \Omega_{\alpha'_m} = \hat{\Omega}_{\alpha}^{(\text{biased})} - (\Gamma^{-1})_{\alpha\alpha'} \Gamma_{\alpha'\alpha'_m} \Omega_{\alpha'_m}, \quad (2)$$

$$\hat{\Omega}_{\alpha}^{(\text{biased})} = \text{Tr} \left[ (\Gamma^{-1})_{\alpha\alpha'} X_{\alpha'} \right] = \text{Tr} \left[ (\Gamma^{-1})_{\alpha\alpha'} \Gamma_{\alpha'\alpha'_m} \Omega_{\alpha'_m} \right]. \quad (3)$$

where  $\text{Tr}$  denotes the trace over the indices  $\alpha, \alpha_m$ .

<sup>5</sup> This is confirmed from the results in table III. The most biased results appear in the analyses for two and three components that miss three or two components, respectively.

where  $\Omega_{\alpha}$  and  $\Omega_{\alpha_m}$  are the power-law injection amplitudes for the  $\alpha$  and  $\alpha_m$  components, respectively, and  $w_{\alpha}$  and  $w_{\alpha_m}$  are the corresponding weight functions.

b. Signal on top of O3 data

The total power-law injection spectrum is then given by

$$\hat{\Omega}_{O3}(f) = \hat{\Omega}_{O3}(f) + \hat{\Omega}_{O3}(f) \quad (4)$$

where  $\hat{\Omega}_{O3}(f)$  is the O3 data and  $\hat{\Omega}_{O3}(f)$  is the signal.

2. Power-law injections: three different-intensity SGWBs

The power-law injection spectrum is then given by

$$\Omega_{\alpha} = 2^{-3} \times \Omega_{2/3} \quad \Omega_{\alpha} = 2^{-5} \times \Omega_{2/3} \quad (5)$$

	$\hat{\Omega}_0 = 1 \times 10^{-6}$	$\hat{\Omega}_{2/3} = 1 \times 10^{-6}$	$\hat{\Omega}_2 = 1 \times 10^{-6}$	$\hat{\Omega}_3 = 1 \times 10^{-6}$	$\hat{\Omega}_4 = 1 \times 10^{-6}$
$\alpha = \{0\}$	$(1.9420 \pm 0.0008) \times 10^{-5}$	-	-	-	-
$\alpha = \{2/3\}$	-	$(1.8066 \pm 0.0006) \times 10^{-5}$	-	-	-
$\alpha = \{2\}$	-	-	$(1.2519 \pm 0.0002) \times 10^{-5}$	-	-
$\alpha = \{3\}$	-	-	-	$(5.6650 \pm 0.0008) \times 10^{-6}$	-
$\alpha = \{4\}$	-	-	-	-	$(1.2262 \pm 0.0002) \times 10^{-6}$
$\alpha = \{0, 2/3\}$	$(-1.5621 \pm 0.0004) \times 10^{-4}$	$(1.3276 \pm 0.0003) \times 10^{-4}$	-	-	-
$\alpha = \{0, 2\}$	$(-3.595 \pm 0.001) \times 10^{-5}$	-	$(2.1765 \pm 0.0004) \times 10^{-5}$	-	-
$\alpha = \{0, 3\}$	$(-9.516 \pm 0.009) \times 10^{-6}$	-	-	$(6.205 \pm 0.001) \times 10^{-6}$	-
$\alpha = \{0, 4\}$	$(7.665 \pm 0.008) \times 10^{-6}$	-	-	-	$(1.1886 \pm 0.0002) \times 10^{-6}$
$\alpha = \{2/3, 2\}$	-	$(-3.874 \pm 0.001) \times 10^{-5}$	$(2.7240 \pm 0.0005) \times 10^{-5}$	-	-
$\alpha = \{2/3, 3\}$	-	$(-9.227 \pm 0.007) \times 10^{-6}$	-	$(6.513 \pm 0.001) \times 10^{-6}$	-
$\alpha = \{2/3, 4\}$	-	$(6.305 \pm 0.006) \times 10^{-6}$	-	-	$(1.1696 \pm 0.0002) \times 10^{-6}$
$\alpha = \{2, 3\}$	-	-	$(-9.976 \pm 0.005) \times 10^{-6}$	$(8.751 \pm 0.002) \times 10^{-6}$	-
$\alpha = \{2, 4\}$	-	-	$(3.521 \pm 0.003) \times 10^{-6}$	-	$(1.0827 \pm 0.0002) \times 10^{-6}$
$\alpha = \{3, 4\}$	-	-	-	$(1.819 \pm 0.002) \times 10^{-6}$	$(9.141 \pm 0.003) \times 10^{-7}$
$\alpha = \{0, 2/3, 2\}$	$(2.253 \pm 0.001) \times 10^{-4}$	$(-2.5345 \pm 0.0009) \times 10^{-4}$	$(5.086 \pm 0.001) \times 10^{-5}$	-	-
$\alpha = \{0, 2/3, 3\}$	$(9.418 \pm 0.007) \times 10^{-5}$	$(-8.525 \pm 0.005) \times 10^{-5}$	-	$(8.154 \pm 0.002) \times 10^{-6}$	-
$\alpha = \{0, 2/3, 4\}$	$(-2.188 \pm 0.005) \times 10^{-5}$	$(2.278 \pm 0.004) \times 10^{-5}$	-	-	$(1.1288 \pm 0.0002) \times 10^{-6}$
$\alpha = \{0, 2, 3\}$	$(2.918 \pm 0.002) \times 10^{-5}$	-	$(-2.584 \pm 0.001) \times 10^{-5}$	$(1.2001 \pm 0.0003) \times 10^{-5}$	-
$\alpha = \{0, 2, 4\}$	$(-9.7 \pm 0.2) \times 10^{-7}$	-	$(3.839 \pm 0.006) \times 10^{-6}$	-	$(1.0745 \pm 0.0002) \times 10^{-6}$
$\alpha = \{0, 3, 4\}$	$(3.35 \pm 0.01) \times 10^{-6}$	-	-	$(1.385 \pm 0.002) \times 10^{-6}$	$(9.722 \pm 0.004) \times 10^{-7}$
$\alpha = \{2/3, 2, 3\}$	-	$(3.603 \pm 0.002) \times 10^{-5}$	$(-3.527 \pm 0.002) \times 10^{-5}$	$(1.3262 \pm 0.0003) \times 10^{-5}$	-
$\alpha = \{2/3, 2, 4\}$	-	$(-1.20 \pm 0.02) \times 10^{-6}$	$(4.076 \pm 0.008) \times 10^{-6}$	-	$(1.0708 \pm 0.0003) \times 10^{-6}$
$\alpha = \{2/3, 3, 4\}$	-	$(2.904 \pm 0.009) \times 10^{-6}$	-	$(1.255 \pm 0.002) \times 10^{-6}$	$(9.848 \pm 0.004) \times 10^{-7}$
$\alpha = \{2, 3, 4\}$	-	-	$(2.599 \pm 0.008) \times 10^{-6}$	$(5.32 \pm 0.04) \times 10^{-7}$	$(1.0289 \pm 0.0005) \times 10^{-6}$
$\alpha = \{0, 2/3, 2, 3\}$	$(-1.525 \pm 0.001) \times 10^{-4}$	$(2.045 \pm 0.002) \times 10^{-4}$	$(-7.061 \pm 0.004) \times 10^{-5}$	$(1.7369 \pm 0.0005) \times 10^{-5}$	-
$\alpha = \{0, 2/3, 2, 4\}$	$(1.18 \pm 0.01) \times 10^{-5}$	$(-1.30 \pm 0.01) \times 10^{-5}$	$(5.68 \pm 0.02) \times 10^{-6}$	-	$(1.054 \pm 0.0003) \times 10^{-6}$
$\alpha = \{0, 2/3, 3, 4\}$	$(-1.50 \pm 0.08) \times 10^{-6}$	$(4.18 \pm 0.07) \times 10^{-6}$	-	$(1.202 \pm 0.004) \times 10^{-6}$	$(9.898 \pm 0.005) \times 10^{-7}$
$\alpha = \{0, 2, 3, 4\}$	$(1.82 \pm 0.03) \times 10^{-6}$	-	$(1.29 \pm 0.02) \times 10^{-6}$	$(9.44 \pm 0.07) \times 10^{-7}$	$(1.0027 \pm 0.0006) \times 10^{-6}$
$\alpha = \{2/3, 2, 3, 4\}$	-	$(2.21 \pm 0.03) \times 10^{-6}$	$(6.6 \pm 0.3) \times 10^{-7}$	$(1.063 \pm 0.009) \times 10^{-6}$	$(9.970 \pm 0.007) \times 10^{-7}$
$\alpha = \{0, 2/3, 2, 3, 4\}$	$(1.0 \pm 0.2) \times 10^{-6}$	$(1.0 \pm 0.3) \times 10^{-6}$	$(1.00 \pm 0.07) \times 10^{-6}$	$(1.00 \pm 0.02) \times 10^{-6}$	$(1.0000 \pm 0.0009) \times 10^{-6}$

TABLE III. Estimators from the multi-components analysis in the 20 – 1726 Hz band for the different combinations of the five spectral indices for the signal-only, power-law injection data set, with  $\Omega_\alpha = 10^{-6}$ . Horizontal lines divide the table in regions where a fixed number of components is considered for the analysis.

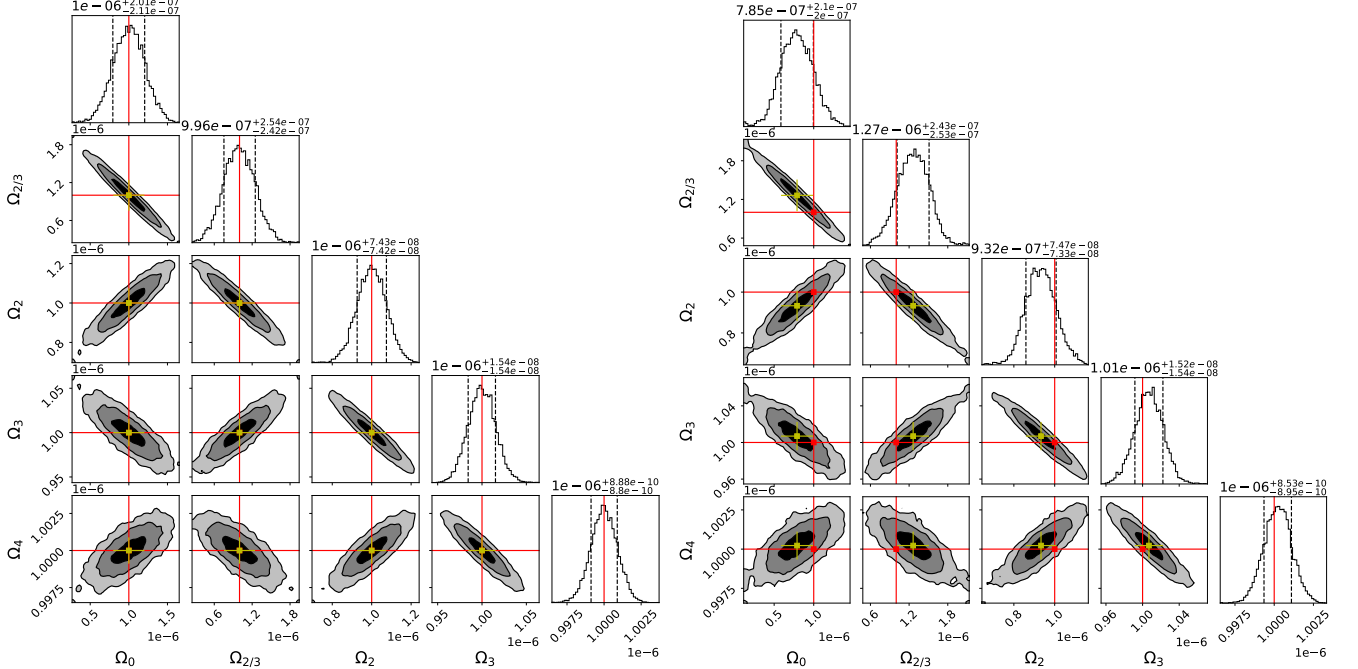


FIG. 4. Parameter estimation results for the set of the power-law injections in the 20 – 1726 Hz frequency range, with  $\Omega_\alpha = 1 \times 10^{-6}$ ,  $\alpha = 0, 2/3, 2, 3, 4$ , for the signal-only case (left panel) and on top of O3 data (right panel). Contour plots show the  $1\sigma$ ,  $2\sigma$ , and  $3\sigma$  credible areas (black, grey, light grey, respectively). The red lines denote the injected values, while the yellow error bars represent the  $1\sigma$  uncertainty of the  $\Omega_\alpha$  estimators from the joint analysis. The dashed black lines in the histogram panels delimit the  $1\sigma$  region of the estimated parameters.

	$\hat{\Omega}_0 = 1 \times 10^{-6}$	$\hat{\Omega}_{2/3} = 1 \times 10^{-6}$	$\hat{\Omega}_2 = 1 \times 10^{-6}$	$\hat{\Omega}_3 = 1 \times 10^{-6}$	$\hat{\Omega}_4 = 1 \times 10^{-6}$
$\alpha = \{0\}$	$(1.9421 \pm 0.0008) \times 10^{-5}$	-	-	-	-
$\alpha = \{2/3\}$	-	$(1.8066 \pm 0.0006) \times 10^{-5}$	-	-	-
$\alpha = \{2\}$	-	-	$(1.2517 \pm 0.0002) \times 10^{-5}$	-	-
$\alpha = \{3\}$	-	-	-	$(5.6644 \pm 0.0008) \times 10^{-6}$	-
$\alpha = \{4\}$	-	-	-	-	$(1.2263 \pm 0.0002) \times 10^{-6}$
$\alpha = \{0, 2/3\}$	$(-1.5616 \pm 0.0004) \times 10^{-4}$	$(1.3272 \pm 0.0003) \times 10^{-4}$	-	-	-
$\alpha = \{0, 2\}$	$(-3.593 \pm 0.001) \times 10^{-5}$	-	$(2.1759 \pm 0.0004) \times 10^{-5}$	-	-
$\alpha = \{0, 3\}$	$(-9.510 \pm 0.009) \times 10^{-6}$	-	-	$(6.204 \pm 0.001) \times 10^{-6}$	-
$\alpha = \{0, 4\}$	$(7.666 \pm 0.008) \times 10^{-6}$	-	-	-	$(1.1887 \pm 0.0002) \times 10^{-6}$
$\alpha = \{2/3, 2\}$	-	$(-3.873 \pm 0.001) \times 10^{-5}$	$(2.7233 \pm 0.0005) \times 10^{-5}$	-	-
$\alpha = \{2/3, 3\}$	-	$(-9.223 \pm 0.007) \times 10^{-6}$	-	$(6.512 \pm 0.001) \times 10^{-6}$	-
$\alpha = \{2/3, 4\}$	-	$(6.305 \pm 0.006) \times 10^{-6}$	-	-	$(1.1696 \pm 0.0002) \times 10^{-6}$
$\alpha = \{2, 3\}$	-	-	$(-9.975 \pm 0.005) \times 10^{-6}$	$(8.750 \pm 0.002) \times 10^{-6}$	-
$\alpha = \{2, 4\}$	-	-	$(3.518 \pm 0.003) \times 10^{-6}$	-	$(1.0828 \pm 0.0002) \times 10^{-6}$
$\alpha = \{3, 4\}$	-	-	-	$(1.817 \pm 0.002) \times 10^{-6}$	$(9.146 \pm 0.003) \times 10^{-7}$
$\alpha = \{0, 2/3, 2\}$	$(2.2532 \pm 0.001) \times 10^{-4}$	$(-2.5342 \pm 0.0009) \times 10^{-4}$	$(5.085 \pm 0.001) \times 10^{-5}$	-	-
$\alpha = \{0, 2/3, 3\}$	$(9.423 \pm 0.007) \times 10^{-5}$	$(-8.528 \pm 0.005) \times 10^{-5}$	-	$(8.154 \pm 0.002) \times 10^{-6}$	-
$\alpha = \{0, 2/3, 4\}$	$(-2.181 \pm 0.005) \times 10^{-5}$	$(2.273 \pm 0.004) \times 10^{-5}$	-	-	$(1.1290 \pm 0.0002) \times 10^{-6}$
$\alpha = \{0, 2, 3\}$	$(2.921 \pm 0.002) \times 10^{-5}$	-	$(-2.585 \pm 0.001) \times 10^{-5}$	$(1.2004 \pm 0.0003) \times 10^{-5}$	-
$\alpha = \{0, 2, 4\}$	$(-9.5 \pm 0.2) \times 10^{-7}$	-	$(3.828 \pm 0.006) \times 10^{-6}$	-	$(1.0748 \pm 0.0002) \times 10^{-6}$
$\alpha = \{0, 3, 4\}$	$(3.36 \pm 0.01) \times 10^{-6}$	-	-	$(1.381 \pm 0.002) \times 10^{-6}$	$(9.729 \pm 0.004) \times 10^{-7}$
$\alpha = \{2/3, 2, 3\}$	-	$(3.607 \pm 0.002) \times 10^{-5}$	$(-3.529 \pm 0.002) \times 10^{-5}$	$(1.3266 \pm 0.0003) \times 10^{-5}$	-
$\alpha = \{2/3, 2, 4\}$	-	$(-1.17 \pm 0.02) \times 10^{-6}$	$(4.060 \pm 0.008) \times 10^{-6}$	-	$(1.0713 \pm 0.0003) \times 10^{-6}$
$\alpha = \{2/3, 3, 4\}$	-	$(2.917 \pm 0.009) \times 10^{-6}$	-	$(1.250 \pm 0.002) \times 10^{-6}$	$(9.856 \pm 0.004) \times 10^{-7}$
$\alpha = \{2, 3, 4\}$	-	-	$(2.611 \pm 0.008) \times 10^{-6}$	$(5.24 \pm 0.04) \times 10^{-7}$	$(1.0299 \pm 0.0005) \times 10^{-6}$
$\alpha = \{0, 2/3, 2, 3\}$	$(-1.528 \pm 0.001) \times 10^{-4}$	$(2.048 \pm 0.002) \times 10^{-4}$	$(-7.069 \pm 0.004) \times 10^{-5}$	$(1.7380 \pm 0.0005) \times 10^{-5}$	-
$\alpha = \{0, 2/3, 2, 4\}$	$(1.17 \pm 0.01) \times 10^{-5}$	$(-1.29 \pm 0.01) \times 10^{-5}$	$(5.64 \pm 0.02) \times 10^{-6}$	-	$(1.0547 \pm 0.0003) \times 10^{-6}$
$\alpha = \{0, 2/3, 3, 4\}$	$(-1.55 \pm 0.08) \times 10^{-6}$	$(4.23 \pm 0.07) \times 10^{-6}$	-	$(1.196 \pm 0.004) \times 10^{-6}$	$(9.907 \pm 0.005) \times 10^{-7}$
$\alpha = \{0, 2, 3, 4\}$	$(1.82 \pm 0.03) \times 10^{-6}$	-	$(1.3 \pm 0.02) \times 10^{-6}$	$(9.37 \pm 0.07) \times 10^{-7}$	$(1.0036 \pm 0.0006) \times 10^{-6}$
$\alpha = \{2/3, 2, 3, 4\}$	-	$(2.21 \pm 0.03) \times 10^{-6}$	$(6.7 \pm 0.3) \times 10^{-7}$	$(1.057 \pm 0.009) \times 10^{-6}$	$(9.979 \pm 0.007) \times 10^{-7}$
$\alpha = \{0, 2/3, 2, 3, 4\}$	$(7.9 \pm 2.0) \times 10^{-7}$	$(1.3 \pm 0.2) \times 10^{-6}$	$(9.3 \pm 0.7) \times 10^{-7}$	$(1.01 \pm 0.02) \times 10^{-6}$	$(1.0002 \pm 0.0009) \times 10^{-6}$

TABLE IV. Estimators from the multi-components analysis in the 20 – 1726 Hz band for the different combinations of the five spectral indices for power-law injection data set on top of the O3 data, with  $\Omega_\alpha = 10^{-6}$ . Horizontal lines divide the table in regions where a fixed number of components is considered for the analysis.

Fig. 6. Multi-  
component  
analysis of  
the  
 $\Omega_{2/3}$  vs  
the  
estimator  
for  
 $\alpha = \{0, 2/3, 2, 3, 4\}$

Fig. 6. Multi-  
component  
analysis of  
the  
 $\Omega_{2/3}$  vs  
the  
estimator  
for  
 $\alpha = \{0, 2/3, 2, 3, 4\}$

a. Signal-only case with O3 rescaled sensitivity

Fig. 6. Multi-  
component  
analysis of  
the  
 $\Omega_{2/3}$  vs  
the  
estimator  
for  
 $\alpha = \{0, 2/3, 2, 3, 4\}$

Fig. 6. Multi-  
component  
analysis of  
the  
 $\Omega_{2/3}$  vs  
the  
estimator  
for  
 $\alpha = \{0, 2/3, 2, 3, 4\}$

Fig. 6. Multi-  
component  
analysis of  
the  
 $\Omega_{2/3}$  vs  
the  
estimator  
for  
 $\alpha = \{0, 2/3, 2, 3, 4\}$

Fig. 6. Multi-  
component  
analysis of  
the  
 $\Omega_{2/3}$  vs  
the  
estimator  
for  
 $\alpha = \{0, 2/3, 2, 3, 4\}$

Fig. 6. Multi-  
component  
analysis of  
the  
 $\Omega_{2/3}$  vs  
the  
estimator  
for  
 $\alpha = \{0, 2/3, 2, 3, 4\}$

Fig. 6. Multi-  
component  
analysis of  
the  
 $\Omega_{2/3}$  vs  
the  
estimator  
for  
 $\alpha = \{0, 2/3, 2, 3, 4\}$

<sup>6</sup> However, this may no longer be true if  $\Omega_2 = 10^{-2} - 10^{-1} \times \Omega_{2/3}$ , since the bias in the single-component estimator increases by a factor of 10 – 100, passing from 0.22% in table V to 2.2% – 22%.



	$\hat{\Omega}_0 = 0$	$\hat{\Omega}_{2/3} = 1 \times 10^{-9}$	$\hat{\Omega}_2 = 1 \times 10^{-12}$	$\hat{\Omega}_3 = 0$	$\hat{\Omega}_4 = 1 \times 10^{-14}$
$\alpha = \{0\}$	$(1.32561 \pm 0.00008) \times 10^{-9}$	-	-	-	-
$\alpha = \{2/3\}$	-	$(1.00219 \pm 0.00006) \times 10^{-9}$	-	-	-
$\alpha = \{2\}$	-	-	$(3.8106 \pm 0.0002) \times 10^{-10}$	-	-
$\alpha = \{3\}$	-	-	-	$(9.2225 \pm 0.0008) \times 10^{-11}$	-
$\alpha = \{4\}$	-	-	-	-	$(9.041 \pm 0.002) \times 10^{-12}$
$\alpha = \{0, 2/3\}$	$(-8.7 \pm 0.4) \times 10^{-12}$	$(1.0086 \pm 0.0003) \times 10^{-9}$	-	-	-
$\alpha = \{0, 2\}$	$(1.0306 \pm 0.0001) \times 10^{-9}$	-	$(1.1598 \pm 0.0004) \times 10^{-10}$	-	-
$\alpha = \{0, 3\}$	$(1.21771 \pm 0.00009) \times 10^{-9}$	-	-	$(2.314 \pm 0.001) \times 10^{-11}$	-
$\alpha = \{0, 4\}$	$(1.29924 \pm 0.00008) \times 10^{-9}$	-	-	-	$(2.666 \pm 0.002) \times 10^{-12}$
$\alpha = \{2/3, 2\}$	-	$(9.996 \pm 0.001) \times 10^{-10}$	$(1.22 \pm 0.05) \times 10^{-12}$	-	-
$\alpha = \{2/3, 3\}$	-	$(1.00116 \pm 0.00007) \times 10^{-9}$	-	$(2.4 \pm 0.1) \times 10^{-13}$	-
$\alpha = \{2/3, 4\}$	-	$(1.00184 \pm 0.00006) \times 10^{-9}$	-	-	$(3.4 \pm 0.2) \times 10^{-14}$
$\alpha = \{2, 3\}$	-	-	$(7.0273 \pm 0.0005) \times 10^{-10}$	$(-1.2513 \pm 0.0002) \times 10^{-10}$	-
$\alpha = \{2, 4\}$	-	-	$(4.6276 \pm 0.0003) \times 10^{-10}$	-	$(-9.831 \pm 0.002) \times 10^{-12}$
$\alpha = \{3, 4\}$	-	-	-	$(1.948 \pm 0.0002) \times 10^{-10}$	$(-2.438 \pm 0.0003) \times 10^{-11}$
$\alpha = \{0, 2/3, 2\}$	$(2.0 \pm 1.0) \times 10^{-12}$	$(9.977 \pm 0.009) \times 10^{-10}$	$(1.4 \pm 0.1) \times 10^{-12}$	-	-
$\alpha = \{0, 2/3, 3\}$	$(-2.5 \pm 0.7) \times 10^{-12}$	$(1.0032 \pm 0.0005) \times 10^{-9}$	-	$(2.0 \pm 0.2) \times 10^{-13}$	-
$\alpha = \{0, 2/3, 4\}$	$(-5.9 \pm 0.5) \times 10^{-12}$	$(1.0063 \pm 0.0004) \times 10^{-9}$	-	-	$(2.3 \pm 0.2) \times 10^{-14}$
$\alpha = \{0, 2, 3\}$	$(8.887 \pm 0.002) \times 10^{-10}$	-	$(2.196 \pm 0.001) \times 10^{-10}$	$(-2.613 \pm 0.003) \times 10^{-11}$	-
$\alpha = \{0, 2, 4\}$	$(9.800 \pm 0.002) \times 10^{-10}$	-	$(1.4192 \pm 0.0006) \times 10^{-10}$	-	$(-1.555 \pm 0.002) \times 10^{-12}$
$\alpha = \{0, 3, 4\}$	$(1.1619 \pm 0.0001) \times 10^{-9}$	-	-	$(4.404 \pm 0.002) \times 10^{-11}$	$(-4.217 \pm 0.004) \times 10^{-12}$
$\alpha = \{2/3, 2, 3\}$	-	$(1.0003 \pm 0.0002) \times 10^{-9}$	$(6.4 \pm 1.7) \times 10^{-13}$	$(1.2 \pm 0.3) \times 10^{-13}$	-
$\alpha = \{2/3, 2, 4\}$	-	$(1.0000 \pm 0.0002) \times 10^{-9}$	$(1.00 \pm 0.08) \times 10^{-12}$	-	$(1.0 \pm 0.3) \times 10^{-14}$
$\alpha = \{2/3, 3, 4\}$	-	$(1.00106 \pm 0.00009) \times 10^{-9}$	-	$(2.9 \pm 0.2) \times 10^{-13}$	$(-8.5 \pm 3.8) \times 10^{-15}$
$\alpha = \{2, 3, 4\}$	-	-	$(8.7956 \pm 0.0008) \times 10^{-10}$	$(-2.40705 \pm 0.0004) \times 10^{-10}$	$(1.4469 \pm 0.0005) \times 10^{-11}$
$\alpha = \{0, 2/3, 2, 3\}$	$(-1.5 \pm 1.5) \times 10^{-12}$	$(1.002 \pm 0.002) \times 10^{-9}$	$(2.8 \pm 3.8) \times 10^{-13}$	$(1.6 \pm 0.5) \times 10^{-13}$	-
$\alpha = \{0, 2/3, 2, 4\}$	$(-0.00 \pm 1.14) \times 10^{-11}$	$(1.000 \pm 0.001) \times 10^{-9}$	$(1.00 \pm 0.17) \times 10^{-12}$	-	$(1.0 \pm 0.3) \times 10^{-14}$
$\alpha = \{0, 2/3, 3, 4\}$	$(-2.5 \pm 0.8) \times 10^{-12}$	$(1.0032 \pm 0.0007) \times 10^{-9}$	-	$(2.0 \pm 0.4) \times 10^{-13}$	$(-2.3 \pm 45.9) \times 10^{-16}$
$\alpha = \{0, 2, 3, 4\}$	$(8.159 \pm 0.003) \times 10^{-10}$	-	$(2.919 \pm 0.002) \times 10^{-10}$	$(-5.559 \pm 0.007) \times 10^{-11}$	$(2.671 \pm 0.006) \times 10^{-12}$
$\alpha = \{2/3, 2, 3, 4\}$	-	$(1.0000 \pm 0.0003) \times 10^{-9}$	$(1.00 \pm 0.29) \times 10^{-12}$	$(0.0 \pm 8.7) \times 10^{-14}$	$(1.00 \pm 0.66) \times 10^{-14}$
$\alpha = \{0, 2/3, 2, 3, 4\}$	$(-0.00 \pm 2.02) \times 10^{-12}$	$(1.000 \pm 0.002) \times 10^{-9}$	$(1.0 \pm 0.7) \times 10^{-12}$	$(0.00 \pm 1.54) \times 10^{-13}$	$(1.00 \pm 0.89) \times 10^{-14}$

TABLE V. Estimators from the multi-components analysis in the 20–1726 Hz band for different spectral-index combinations for the dominant-component, signal-only, power-law injection data set, with  $\Omega_{2/3} = 1 \times 10^{-9}$ ,  $\Omega_2 = 1 \times 10^{-12}$ , and  $\Omega_4 = 1 \times 10^{-14}$ . Horizontal lines divide the table in regions where a fixed number of components is considered for the analysis.

**3. Astrophysical injections**

$\Omega_{2/3} = 1 \times 10^{-9}$ ,  $\Omega_2 = 1 \times 10^{-12}$ ,  $\Omega_4 = 1 \times 10^{-14}$

$\alpha = \{2/3, 2, 3, 4\}$

0.1% injection

$\Omega_{\text{gw}, i}(f)$ ,  $i = 1, \dots, N_{\text{components}}$

$K_{\text{BNS}} \simeq 7.9 \times 10^5 M_{\odot}^{5/3} G^{-3} y^{-1}$

$K_{\text{r-modes}} \simeq 1 \times 10^3$ ,  $K_{\text{magnetars}} \simeq 1 \times 10^{11}$

$\Omega_{\text{ref, BNS}} \simeq 2.12 \times 10^{-7}$ ,  $\Omega_{\text{ref, r-modes}} \simeq 1.69 \times 10^{-7}$

$\Omega_{\text{ref, magnetars}} \simeq 1.9 \times 10^{-8}$

$\alpha = \{0, 2/3, 2, 3, 4\}$

20–1726 Hz band

$\Omega_{\text{ref}} \simeq 100$

**a. Signal-only case using O3 sensitivity**



	$\hat{\Omega}_0$	$\hat{\Omega}_{2/3} = 2.1 \times 10^{-7}$	$\hat{\Omega}_2 = 1.7 \times 10^{-7}$	$\hat{\Omega}_3$	$\hat{\Omega}_4 = 1.8 \times 10^{-8}$
$\alpha = \{0\}$	$(8.66 \pm 0.08) \times 10^{-7}$	-	-	-	-
$\alpha = \{2/3\}$	-	$(7.11 \pm 0.06) \times 10^{-7}$	-	-	-
$\alpha = \{2\}$	-	-	$(3.62 \pm 0.03) \times 10^{-7}$	-	-
$\alpha = \{3\}$	-	-	-	$(1.45 \pm 0.01) \times 10^{-7}$	-
$\alpha = \{4\}$	-	-	-	-	$(4.32 \pm 0.03) \times 10^{-8}$
$\alpha = \{0, 2/3\}$	$(-2.72 \pm 0.05) \times 10^{-6}$	$(2.71 \pm 0.03) \times 10^{-6}$	-	-	-
$\alpha = \{0, 2\}$	$(-1.4 \pm 0.1) \times 10^{-7}$	-	$(4.02 \pm 0.05) \times 10^{-7}$	-	-
$\alpha = \{0, 3\}$	$(3.5 \pm 0.1) \times 10^{-7}$	-	-	$(1.16 \pm 0.01) \times 10^{-7}$	-
$\alpha = \{0, 4\}$	$(5.73 \pm 0.08) \times 10^{-7}$	-	-	-	$(3.26 \pm 0.04) \times 10^{-8}$
$\alpha = \{2/3, 2\}$	-	$(-1.6 \pm 0.1) \times 10^{-7}$	$(4.29 \pm 0.06) \times 10^{-7}$	-	-
$\alpha = \{2/3, 3\}$	-	$(2.94 \pm 0.08) \times 10^{-7}$	-	$(1.06 \pm 0.01) \times 10^{-7}$	-
$\alpha = \{2/3, 4\}$	-	$(4.67 \pm 0.07) \times 10^{-7}$	-	-	$(2.84 \pm 0.04) \times 10^{-8}$
$\alpha = \{2, 3\}$	-	-	$(2.53 \pm 0.07) \times 10^{-7}$	$(4.8 \pm 0.3) \times 10^{-8}$	-
$\alpha = \{2, 4\}$	-	-	$(3.03 \pm 0.04) \times 10^{-7}$	-	$(9.9 \pm 0.6) \times 10^{-9}$
$\alpha = \{3, 4\}$	-	-	-	$(2.60 \pm 0.04) \times 10^{-7}$	$(-4.0 \pm 0.1) \times 10^{-8}$
$\alpha = \{0, 2/3, 2\}$	$(1.5 \pm 0.1) \times 10^{-6}$	$(-1.6 \pm 0.1) \times 10^{-6}$	$(6.1 \pm 0.2) \times 10^{-7}$	-	-
$\alpha = \{0, 2/3, 3\}$	$(7.6 \pm 8.3) \times 10^{-8}$	$(2.3 \pm 0.7) \times 10^{-7}$	-	$(1.08 \pm 0.03) \times 10^{-7}$	-
$\alpha = \{0, 2/3, 4\}$	$(-5.9 \pm 0.7) \times 10^{-7}$	$(9.3 \pm 0.6) \times 10^{-7}$	-	-	$(2.46 \pm 0.06) \times 10^{-8}$
$\alpha = \{0, 2, 3\}$	$(2.6 \pm 0.3) \times 10^{-7}$	-	$(6.7 \pm 2.3) \times 10^{-8}$	$(9.7 \pm 0.6) \times 10^{-8}$	-
$\alpha = \{0, 2, 4\}$	$(1.8 \pm 0.2) \times 10^{-7}$	-	$(2.2 \pm 0.1) \times 10^{-7}$	-	$(1.6 \pm 0.1) \times 10^{-8}$
$\alpha = \{0, 3, 4\}$	$(3.1 \pm 0.2) \times 10^{-7}$	-	-	$(1.35 \pm 0.08) \times 10^{-7}$	$(-5.6 \pm 2.3) \times 10^{-9}$
$\alpha = \{2/3, 2, 3\}$	-	$(3.4 \pm 0.4) \times 10^{-7}$	$(-4.4 \pm 3.4) \times 10^{-8}$	$(1.17 \pm 0.08) \times 10^{-7}$	-
$\alpha = \{2/3, 2, 4\}$	-	$(2.1 \pm 0.3) \times 10^{-7}$	$(1.7 \pm 0.2) \times 10^{-7}$	-	$(1.8 \pm 0.1) \times 10^{-8}$
$\alpha = \{2/3, 3, 4\}$	-	$(3.2 \pm 0.2) \times 10^{-7}$	-	$(9.0 \pm 1.0) \times 10^{-8}$	$(4.5 \pm 2.8) \times 10^{-9}$
$\alpha = \{2, 3, 4\}$	-	-	$(4.9 \pm 0.3) \times 10^{-7}$	$(-1.6 \pm 0.2) \times 10^{-7}$	$(4.2 \pm 0.5) \times 10^{-8}$
$\alpha = \{0, 2/3, 2, 3\}$	$(-4.8 \pm 3.5) \times 10^{-7}$	$(9.7 \pm 4.6) \times 10^{-7}$	$(-2.4 \pm 1.5) \times 10^{-7}$	$(1.5 \pm 0.3) \times 10^{-7}$	-
$\alpha = \{0, 2/3, 2, 4\}$	$(0.004 \pm 2.735) \times 10^{-7}$	$(2.1 \pm 3.3) \times 10^{-7}$	$(1.7 \pm 0.8) \times 10^{-7}$	-	$(1.8 \pm 0.3) \times 10^{-8}$
$\alpha = \{0, 2/3, 3, 4\}$	$(-2.1 \pm 1.8) \times 10^{-7}$	$(5.3 \pm 1.9) \times 10^{-7}$	-	$(6.1 \pm 2.8) \times 10^{-8}$	$(1.1 \pm 0.6) \times 10^{-8}$
$\alpha = \{0, 2, 3, 4\}$	$(1.4 \pm 0.6) \times 10^{-7}$	-	$(2.8 \pm 1.0) \times 10^{-7}$	$(-3.9 \pm 6.2) \times 10^{-8}$	$(2.2 \pm 1.0) \times 10^{-8}$
$\alpha = \{2/3, 2, 3, 4\}$	-	$(2.1 \pm 1.0) \times 10^{-7}$	$(1.7 \pm 1.5) \times 10^{-7}$	$(0.01 \pm 7.84) \times 10^{-8}$	$(1.8 \pm 1.2) \times 10^{-8}$
$\alpha = \{0, 2/3, 2, 3, 4\}$	$(-0.008 \pm 8.945) \times 10^{-7}$	$(2.1 \pm 13.6) \times 10^{-7}$	$(1.7 \pm 7.1) \times 10^{-7}$	$(0.004 \pm 2.563) \times 10^{-7}$	$(1.8 \pm 3.0) \times 10^{-8}$

TABLE VI. Estimators from the multi-components analysis in the 20 – 100 Hz band for the different combinations of the five spectral indices for the astrophysical BNS, r-mode, and magnetar SGWB signal-only injection data set, with injected parameters  $K_{\text{CBC}} = 7.91 \times 10^5 M_{\odot} \text{Gpc}^{-3} \text{yr}^{-1}$ ,  $K_{\text{r-modes}} = 1 \times 10^3$ , and  $K_{\text{magnetars}} = 1 \times 10^{-11} \text{T}^{-1}$ . Horizontal lines divide the table in regions where a fixed number of components is considered for the analysis.

~~https://~~  
~~arxiv.org/~~  
~~abs/~~  
~~2008.00000~~

~~https://~~  
~~arxiv.org/~~  
~~abs/~~  
~~2008.00000~~

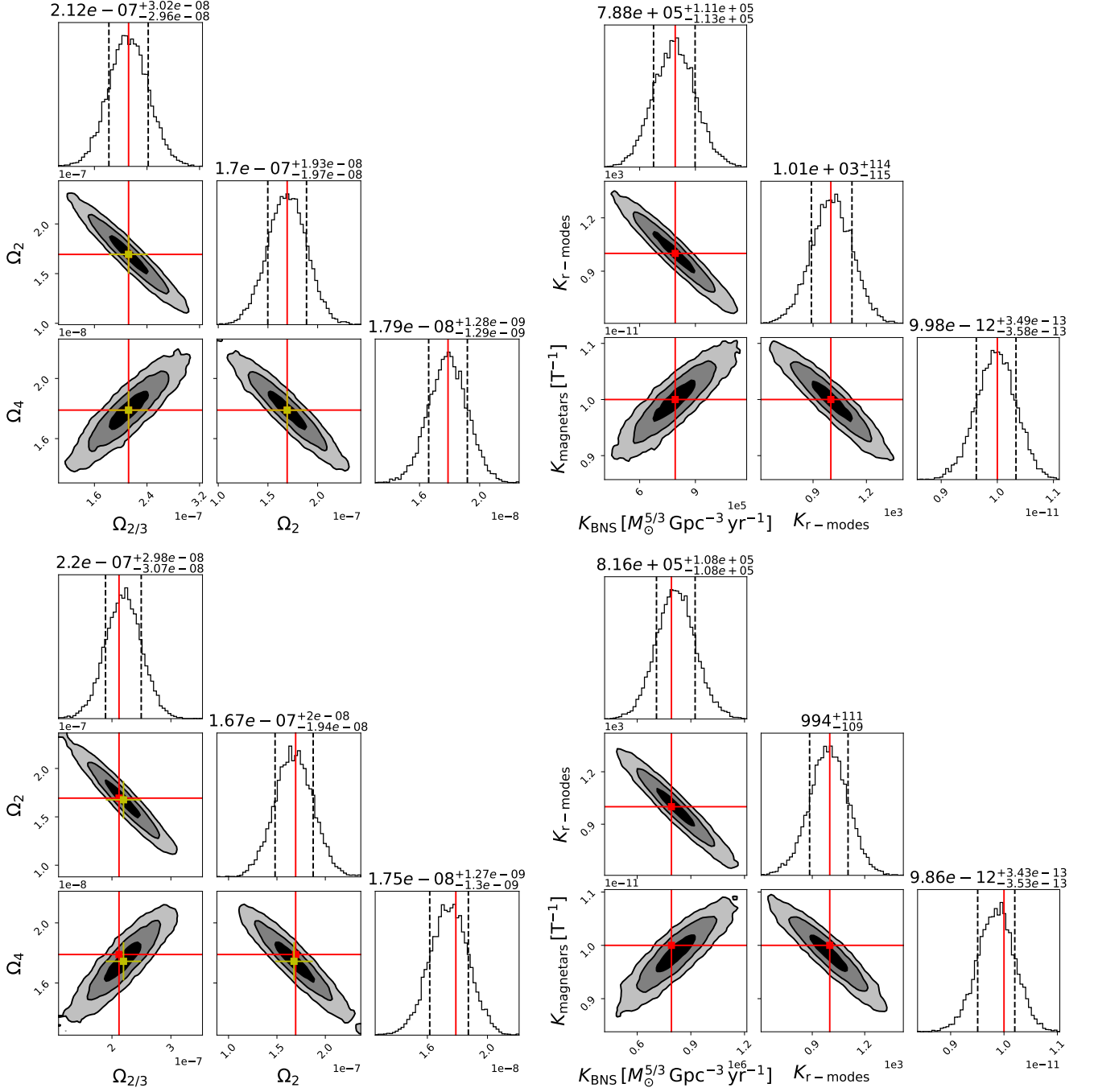


FIG. 6. Results of the parameter estimation for the  $\alpha = 2/3, 2, 4$  combination in the 20 – 100 Hz band for the astrophysical injection for BNS, r-modes, and magnetars SGWBs (top row: signal-only injection; bottom row: injection on top of O3 data). The left panel shows the recovery of the  $\Omega_\alpha$ , while the right panel the injected ensemble parameters. Contour plots show the 1 $\sigma$ , 2 $\sigma$ , and 3 $\sigma$  credible areas (black, grey, light grey, respectively). The red lines denote the injected values, while the yellow error bars represent the 1 $\sigma$  uncertainty of the  $\Omega_\alpha$  estimators from the joint analysis. The dashed black lines in the histogram panels delimit the 1 $\sigma$  region of the estimated parameters.